ELSEVIER

PII: S0032-3861(97)10187-2

Polymer Vol. 39 No. 24 pp. 5987–5998, 1998
0032-3861/98/$ – see front matter

XRD study of the new rigid-rod polymer fibre PIPD

E. A. Klop* and M. Lammers†
Akzo Nobel Central Research, P.O. Box 9300, 6800 SB Arnhem, The Netherlands
(Received 2 September 1997; accepted 24 September 1997)

The new rigid-rod polymer fibre PIPD was studied using wide angle X-ray scattering. The crystal structure of as-spun PIPD fibre can be described as a two-dimensionally ordered crystal hydrate. Its equatorial X-ray diffraction pattern was indexed to a non-primitive rectangular unit cell with parameters 16.85, 3.38 Å, containing two polymer chains. Heat treatment initially (i.e. up to 300°C) leads to the loss of water molecules from the structure as was shown by high temperature X-ray diffraction. At sufficiently high temperatures three-dimensional crystalline order is developed, as evidenced by the presence of strong off-axis reflections in the diffraction pattern of the heat-treated fibre. A procedure of unit cell determination was introduced that made it possible to index the latter diffraction pattern and elucidate the three-dimensional packing. The crystal structure of heat-treated PIPD fibre has monoclinic symmetry described by the space group $P2_1/a$. Its cell dimensions are 12.60, 3.48, 12.01 Å, 90.0, 108.6, 90.0° with $\rho_x = 1.77$ g cm^{-3}. The unit cell is non-primitive ($Z = 2$), with chains located at the centre and corners of the rectangular projection cell describing the lateral packing. Neighbouring chains packed along the diagonals of the projection cell are shifted relative to each other in the direction of the *c*-axis (chain axis) by 2.0 Å. This regular *c*-axis shift explains the observed absence of significant meridional scattering from the lower order layer lines of the diffraction pattern. A hydrogen bonding scheme is proposed consisting of intermolecular N–H—O bonds and intramolecular O–H—N bonds. The intermolecular hydrogen bonds form a bi-directional hydrogen bonding network linking each polymer chain to its four axially shifted neighbours. Departures of the latter hydrogen bonding scheme may be present in the form of hydrogen bonded sheets. The proposed hydrogen bonding scheme is consistent with thermal expansion data provided by high temperature XRD. The monoclinic crystal structure with its bi-directional hydrogen bonding network provides a satisfactory explanation for the exceptionally good compression performance of heat-treated PIPD fibre.

(Keywords: rigid-rod polymer fibre; PIPD; X-ray diffraction)

INTRODUCTION

The introduction of the polymers poly (*p*-phenylene benzobisthiazole) (PBZT) and poly (*p*-phenylene benzobisoxazole) (PBO) (*Figure 1*) some 20 yrs ago marked the beginning of the development of extremely rigid polymers intended for lightweight, high performance structural applications[1]. These so-called rigid-rod polymers form liquid crystalline solutions in polyphosphoric acid, which are spun into fibres. The high levels of molecular orientation thus achieved can be further increased by heat treatment, resulting in materials exhibiting a high stiffness and tenacity. The performance of these fibres in compression, however, is limited[2], due to the absence of strong interchain bonding.

Various attempts have been undertaken at improving the compression performance by the introduction of crosslinks between the polymer chains. Sweeney[3] has examined halogenated PBZT fibres as a function of heat treatment time and temperature, taking halogen loss and fibre insolubility as evidence of crosslinking. Some improvement in compression performance was observed, but this was accompanied by a significant loss of mass, which may be associated with the formation of voids and other structural defects. Sahafeyan and Kumar[4] studied the influence of post heat treatment on heat-treated PBZT fibres. Although the post heat treatment resulted in reduced fibre swelling in methanesulfonic acid, no evidence of crosslinking was observed using infrared spectroscopy. The authors conclude that the decrease in swelling may have been a result of increased order and crystallinity rather than significant crosslinking. Mehta *et al.*[5] studied crosslinking in heat-treated methyl pendent PBZT. While some evidence was obtained that methyl groups participate in crosslinking reactions, also a significant loss of methane was observed. Tan *et al.*[6] reported the synthesis and characterization of dihydroxy-PBZT homopolymer and dihydroxy-PBZT/PBZT copolymers. According to these authors, the hydroxyl groups did not improve the compression properties at all. This was attributed to the occurrence of intramolecular hydrogen bonding instead of the intermolecular hydrogen bonding aimed at. In conclusion, attempts at introducing strong interchain bonding in rigid-rod polymers have not been very encouraging so far.

A way out of these problems was found in our laboratory by Sikkema[7] who, in an accompanying paper, reports the synthesis of the novel rigid-rod polymer poly{2,6-diimidazo[4,5-b:4′,5′-e]pyridinylene-1,4(2,5-dihydroxy)phenylene}, or 'PIPD', in the development stage also called 'M5'. The design of this molecule

* To whom correspondence should be addressed
† On leave from ETH Zürich, Institut für Polymere, Universitätstrasse 41, CH-8092, Zürich, Switzerland

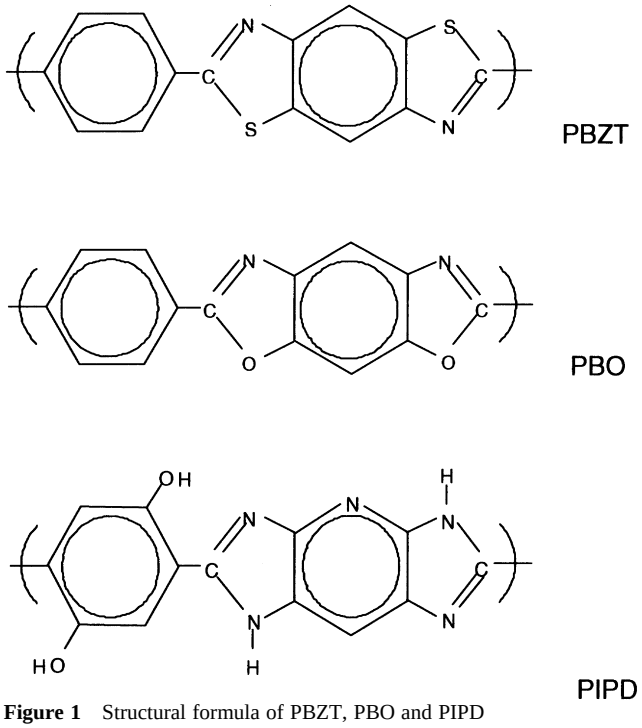

Figure 1 Structural formula of PBZT, PBO and PIPD

(*Figure 1*) combines the high stiffness and tenacity of the rigid-rod polymer family with extensive possibilities to form hydrogen bonds. Fibres spun from a solution of the polymer in polyphosphoric acid exhibit a higher compressive strength than any other polymer fibre. This unique compression performance is intimately linked to the molecular architecture of the PIPD polymer and in particular to the nature of the interchain bonding in PIPD crystallites. In the present paper we use wide angle X-ray scattering to study the structural order in PIPD fibre in order to establish the molecular basis for the outstanding compression performance.

BACKGROUND

X-ray and electron diffraction were used by Roche *et al.*[8] and Odell *et al.*[9] to determine the crystal structure of PBZT. A monoclinic unit cell was found with two chains per unit cell and with the unique axis parallel to the chain axis. Layer line streaking present in the diffraction pattern of PBZT indicates that PBZT crystallites have only two-dimensional crystalline order, i.e. the polymer chains are parallel and regularly packed but they exhibit translational axial disorder. TEM bright-field imaging indicated that limited three-dimensional order may be present[10].

Diffraction patterns of PBO fibre show layer line streaking indicative of axial disorder similar to PBZT. However, with increasing heat treatment the scattering becomes more localized and an off-meridian reflection on the second layer line becomes well-defined and intense. These observations point to the development of three-dimensional crystalline order in the heat-treated PBO fibre[11,12]. TEM bright-field lattice imaging of heat-treated PBO was reported by Adams *et al.*[13]. Using X-ray diffraction, Fratini *et al.*[14] determined a non-primitive monoclinic unit cell with two chains per cell. They proposed a model in which neighbouring polymer chains packed side by side are displaced by discrete axial translations of $\pm 1/10c$ and $\pm 1/2c$ (c being the unit cell axis parallel to the polymer chains). Using selected area electron diffraction Martin and Thomas[12] observed single crystal texturing in thin PBO films which made it possible to index the intense off-meridian reflection on the second layer line. This indexing, which did not coincide with that by Fratini *et al.*[14], led to the conclusion that neighbouring chains packed side by side are shifted by random axial translations of $\pm 1/4c$ with respect to one another, instead of $\pm 1/10c$ and $\pm 1/2c$. A molecular mechanics simulation of the PBO crystal structure was presented by Martin[15] in a study on the geometry and properties of intermolecular twist defects that may exist in extended chain polymers.

EXPERIMENTAL

Polymerization and fibre spinning

The PIPD polymer was prepared from 2,3,5,6-tetra-aminopyridine (TAP) and 2,5-dihydroxyterephthalic acid (DHTA) via the TAP.DHTA 1:1 salt, according to the description given by Sikkema[7]. The salt was dissolved in polyphosphoric acid (PPA) resulting in material with η_{rel} in the 20–50 range. PIPD fibres were directly spun from the polymerization solution at temperatures above 160°C and at a concentration of 18 wt% PIPD in solution. The air gap spinning technique was used with a draw-down ratio in the range 5–15, yielding filaments of about 10 μm diameter. After coagulation in water at room temperature, the remaining PPA was removed in a separate washing stage, and dried at mild temperatures. The as-spun fibre was subsequently heat-treated at temperatures above 400°C for about 20 s under tension in a nitrogen atmosphere[16]. During heat treatment, the metallic blue colour of the as-spun fibre changes hardly.

The PBO fibre that was used for purposes of comparison was produced according to the description in the literature[1].

X-ray diffraction

X-ray diffraction patterns were recorded on film using an evacuated point-collimated flat-plate camera (Statton) with graphite-monochromated CuKα radiation. A Siemens D5000 diffractometer with a primary germanium monochromator was employed to measure equatorial and meridional fibre diffraction patterns in symmetric transmission geometry at room temperature. Above room temperature equatorial diffraction patterns were measured using a Siemens D5000 diffractometer in reflection geometry equipped with an Anton Paar HTK10 hot stage.

Model building and simulation of X-ray diffraction patterns were performed using the Cerius2 software (version 2.0) from Molecular Simulations. The Lorentz and polarization corrections are included in the calculated intensities. The crystallite size, temperature factor, and the degree of arcing due to crystallite desorientation were chosen to match the observed X-ray diffraction patterns.

XRD ANALYSIS OF HEAT-TREATED PIPD FIBRE

Figure 2a shows the flat-plate X-ray diffraction pattern of heat-treated (HT) PIPD fibre. The diffraction pattern exhibits equatorial scattering indicative of lateral packing of PIPD molecules. The polymer chains are well-oriented along the fibre axis. The crystalline perfection of PIPD fibres, like that of other rigid-rod fibres such as PBO, is considerably lower compared to the crystalline perfection of e.g. PPTA fibre, which shows a far greater number of well-defined reflections. The layer line streaking that is observed

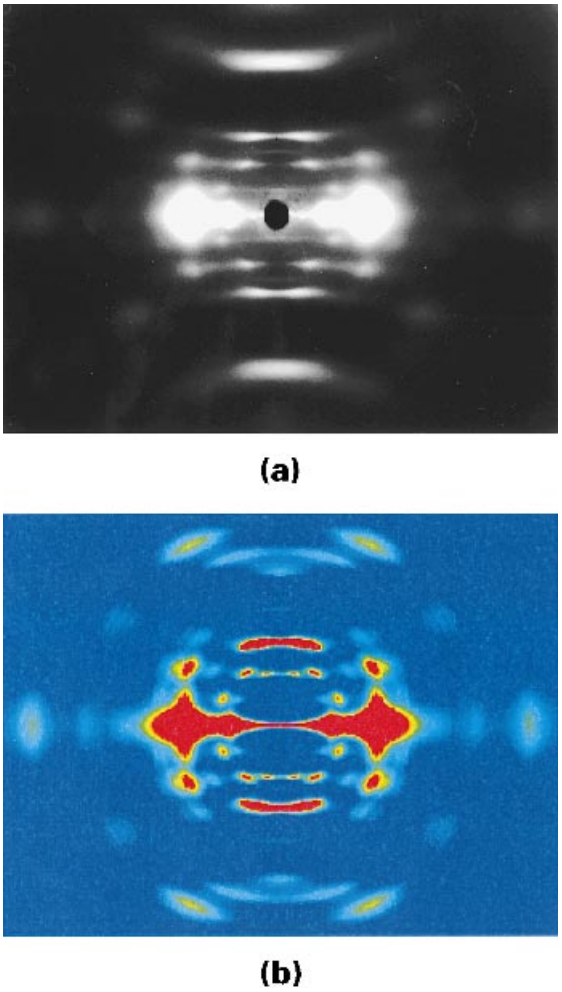

Figure 2 Flat plate X-ray diffraction pattern of HT PIPD fibre, (a) observed, (b) calculated (based on the monoclinic model)

points to some axial disorder, a common characteristic of rigid-rod fibres. A striking and distinctive feature of the PIPD diffraction pattern is the presence of strong off-meridian reflections on the first three layer lines, consistent with three-dimensional crystalline order. A second distinctive feature is the absence of significant meridional scattering from the low order layer lines. The investigation of the structural implications of the latter two observations will be one of the principal subjects of the present study.

First, we will examine more closely the meridional diffraction pattern of HT PIPD shown in *Figure 3a*. The fibre period c deduced from this diffraction pattern was found to be 12.01 Å, the polymer chains being parallel to the c-axis. This repeat closely corresponds to the chemical repeat of the PIPD polymer as determined from model building and is identical to the repeat obtained from the meridional diffraction pattern of HT PBO also shown in *Figure 3a*. A comparison of the diffraction patterns in *Figure 3a* shows that the intensities of scattering are similar at higher diffraction angles, reflecting the similarity in molecular structure of the two polymers. A dramatic difference in intensity is observed in the low angle region of the diffraction patterns, where the intensity for $l = 1$, 3, and 4 is much lower for PIPD than for PBO. The absence of significant scattering in this region of the meridian, already noted on the flat-plate diffraction pattern in *Figure 2a*, suggests that the *ab*-plane of the unit cell of PIPD is *not perpendicular* to the c-axis.

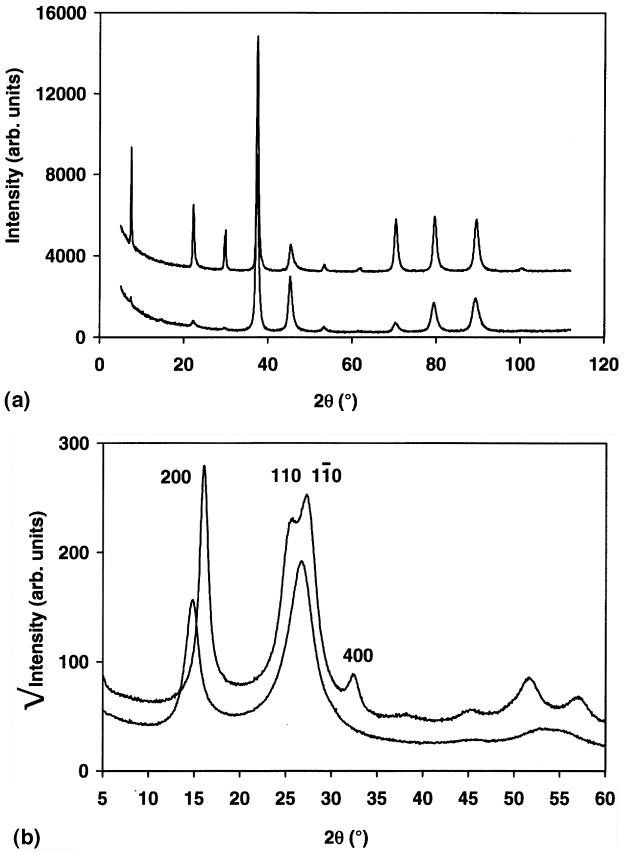

Figure 3 X-ray scattering of HT PIPD fibre (bottom curve) and HT PBO fibre (upper curve) in symmetric transmission geometry, (a) meridional, (b) equatorial

Lateral crystal structure

Now we will restrict our attention to the two-dimensional unit cell corresponding to the lateral packing of the polymer chains, i.e. to the projection of the three-dimensional unit cell on a plane perpendicular to the c-axis (called c-axis projection in the sequel). This projection unit cell was determined from the equatorial diffraction pattern of HT PIPD shown in *Figure 3b*. Two strong equatorial reflections are observed at spacings of 5.98 Å and 3.34 Å, respectively, whereas several weak reflections are observed at smaller spacings. These reflections can be indexed on the basis of a primitive projection unit cell with parameters $a = 6.22$ Å, $b = 3.48$ Å, $\gamma = 106.2°$, which will be referred to as unit cell I_p. As the short diagonal of this unit cell is exactly equal in length to the a-axis, the reflections can also be indexed on a rectangular projection unit cell with dimensions $a = 11.94$ Å, $b = 3.48$ Å (unit cell II_p). Polymer chains are located at the centre and corners of the latter non-primitive unit cell which is obtained from the former by the transformation $\mathbf{a}' = 2\mathbf{a} + \mathbf{b}$ (with **b** and **c** unchanged).

The equatorial diffraction pattern of HT PBO (*Figure 3b*) differs from that of HT PIPD. In contrast to PIPD, the projection unit cell of PBO is not rectangular but oblique, as is directly evident from the splitting of the 3.34 Å reflection into separate 110 and 1$\bar{1}$0 reflections. The PBO unit cell is somewhat smaller in the a direction, as can be concluded from the smaller 200 spacing (5.52 *versus* 5.98 Å). The diffraction pattern of HT PBO was indexed by Fratini *et al.*[14] to a two-chain monoclinic unit cell containing polymer chains at the (x, y) positions (0, 0) and (1/2, 0). After transforming the PBO unit cell via $\mathbf{a}' = \mathbf{a} + \mathbf{b}$ (with **b** and **c** unchanged) so that its polymer chains are located at

(0, 0) and (1/2,1/2), the cell dimensions describing the lateral packing of PBO are $a = 11.07$ Å, $b = 3.54$ Å and $\gamma = 83.0°$, which differ markedly from those of PIPD.

An initial structural model of HT PIPD was constructed using the Cerius2 program by placing a chemical repeat unit at the corner(s) of a primitive unit cell with dimensions $a = 6.22$ Å, $b = 3.48$ Å, $c = 12.01$ Å, $\gamma = 106.2°$. In spite of the rigidity of the PIPD chain some molecular flexibility may be present in the form of limited rotation about the bond between the dihydroxyphenyl fragment and the heterocyclic fragment, i.e. the torsion angle between the two fragments may differ from zero. However, the metallic blue colour of the fibre suggests some degree of conjugation along the molecule requiring a closely planar conformation. In our initial model we started from a completely planar polymer chain which was rotated relative to its chain axis so that the calculated equatorial diffraction pattern matches the observed equatorial diffraction pattern. The model is triclinic (space group *P*1) and its density is calculated to be 1.77 g cm^{-3}, which is in reasonable agreement with the observed density (1.70 g cm^{-3}) obtained via the flotation method. Note that in the model the polymer chains are not shifted relative to each other, since the *ab*-plane of the unit cell is simply the projection unit cell I_p.

Three-dimensional unit cell determination

Unravelling of the three-dimensional crystal structure of PIPD with its interchain interactions is impossible unless the general reflections (i.e. off-equator and off-meridian) can be indexed correctly. The difficulties encountered by Fratini *et al.*[14] in indexing X-ray fibre diffraction data of PBO show that it is not trivial to index fibre diffraction patterns that exhibit only a few general reflections. Standard indexing procedures require considerably more (general) reflections than the few reflections that are actually present in the X-ray fibre diffraction patterns of PBO or PIPD. In favourable cases, additional experimental information may be obtained that simplifies the indexing procedure, such as the information provided by a selected area electron diffraction study of single crystal textured material. This information proved valuable in indexing the diffraction pattern of HT PBO as was shown by Martin and Thomas[12]. Unfortunately, such additional information was not available for PIPD, as single crystal textured material was not observed in a preliminary electron diffraction study[17]. To make matters worse (but interesting), the crystal structure of PIPD may be triclinic, as it was concluded that the *ab*-plane of the unit cell is probably not perpendicular to the *c*-axis. In the face of a possibly triclinic indexing problem with very few reflections the following procedure of unit cell determination and indexing was introduced.

First, the reciprocal cell parameters a^*, b^* and γ^* are deduced from the equatorial diffraction pattern. The distance d^* between reciprocal lattice planes perpendicular to the *c*-axis is simply $d^* = c^{-1}$. Next, indices 00*l* are assigned to a reflection on an (upper) layer line *l* to define the length c^* of the reciprocal space vector $\mathbf{c^*}$ [$c^* = (ld_{00l})^{-1}$]. The projection of $\mathbf{c^*}$ on the reciprocal lattice plane generated by the vectors $\mathbf{a^*}$ and $\mathbf{b^*}$ is c_p^* with

$$c_p^* = \sqrt{c^{*2} - d^{*2}} \tag{1}$$

Now the geometry of the reciprocal lattice is determined except for one parameter, viz. the angle ν between the reciprocal space vectors $\mathbf{a^*}$ and c_p^* (*Figure 4*). Note that

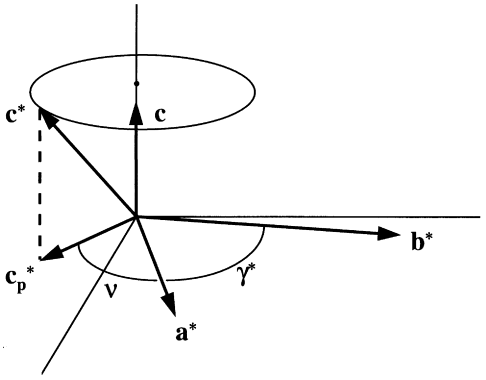

Figure 4 Precession of **c*** about the *c*-axis

$$\begin{aligned} \mathbf{a}^* \cdot \mathbf{c}^* &= \mathbf{a}^* \cdot \mathbf{c}_p^* \\ \mathbf{b}^* \cdot \mathbf{c}^* &= \mathbf{b}^* \cdot \mathbf{c}_p^* \end{aligned} \tag{2}$$

The reciprocal cell parameters α^* and β^* are obtained for a given value of the precession angle ν according to the relationships

$$\begin{aligned} \cos\alpha^* &= \frac{c_p^*}{c^*}\cos(\gamma^* + \nu) \\ \cos\beta^* &= \frac{c_p^*}{c^*}\cos\nu \end{aligned} \tag{3}$$

which follow from the equations (2). Finally, the six reciprocal cell parameters a^*, b^*, c^*, $\alpha^*(\nu)$, $\beta^*(\nu)$ and γ^* are transformed to direct cell parameters $a(\nu)$, $b(\nu)$, c, $\alpha(\nu)$, $\beta(\nu)$ and $\gamma(\nu)$ via inversion of the reciprocal metric tensor. As ν ranges from 0 to 360°, the normal to the *ab*-plane (i.e. **c***) precesses about the *c*-axis (*Figure 4*) and the vectors **a** and **b** change both in magnitude and direction *but their* c*-axis projection does not change*, since a^*, b^* and γ^* are fixed. The unit cell determination problem is now reduced to that of finding the correct precession angle ν.

The latter problem can be solved by matching spacings. The spacing d_{hkl} is expressed in the parameters a^*, b^*, c^*, γ^*, c_p^*, and ν using the equations (2):

$$\begin{aligned} \frac{1}{d_{hkl}^2} = {} & h^2a^{*2} + k^2b^{*2} + l^2c^{*2} + 2hka^*b^*\cos\gamma^* \\ & + 2hla^*c_p^*\cos\nu + 2klb^*c_p^*\cos(\gamma^* + \nu) \end{aligned} \tag{4}$$

In general, plotting d_{hk1} as function of ν for a number of (low order) reflections *hk*1 on the first layer line allows the determination of the parameter ν by matching the spacings calculated via equation (4) with the observed spacings (clearly, this can and should be repeated for other layer lines).

As an alternative to matching spacings, the precession angle can be determined by matching diffraction patterns, i.e. diffraction patterns at different ν-values are calculated and compared with the observed diffraction pattern. The latter approach was adopted in the PIPD indexing problem. Indices 001 were assigned to the well-defined reflection on the first layer line. With ν ranging from 0 to 360° in steps of 2°, direct cell parameters were calculated for each value of ν as outlined above. This way, a list of 180 unit cells, all having the same *c*-axis projection, is generated. For the calculation of the diffraction pattern at a particular ν-value

the coordinates of the starting model are used together with the required cell parameters taken from the list. Hence, the starting model is changed systematically while keeping its *c*-axis projection fixed. Since the diffraction pattern changes gradually with ν, the patterns of only a small subset of the 180 different ν-values have to be inspected.

A satisfactory match between calculated and observed diffraction patterns was found for a precession angle in the 0–4° range. The unit cell corresponding to $\nu = 2°$ was transformed according to $\mathbf{a}' = \mathbf{a} + \mathbf{c}$ (with **b** and **c** unchanged) in order to have angles closer to 90°. Finally, with the indexing now known, the observed spacings of three strong off-axis reflections were employed to determine the tilt of the *ab*-plane more accurately. This resulted in the triclinic unit cell 6.54, 3.48, 12.01 Å, 90.0, 107.9, 105.4° (unit cell I). For reasons that will become apparent in the next section, it is advantageous to describe the structure in the *c*-centered unit cell with dimensions 12.60, 3.48, 12.01 Å, 90.0, 108.6, 90.0° (unit cell II) obtained from the triclinic unit cell after the transformation $\mathbf{a}' = 2\mathbf{a} + \mathbf{b}$ (with **b** and **c** unchanged). By this transformation the primitive projection unit cell I_p is transformed to the rectangular projection unit cell II_p of the centered cell. The resulting indexing is given in *Table 1* together with the observed and calculated diffraction angles.

The indexing described here shows that the *ab*-plane of the unit cell is indeed not perpendicular to the *c*-axis as was already anticipated from the absence of low order meridional scattering. It turns out that neighbouring chains packed along the diagonals of the centered cell show an axial shift $1/2a\cos\beta$, or 2.0 Å, whereas the polymer chains packed face to face along the *b* direction do not.

Final model building

The analysis described so far allows the construction of a triclinic model for HT PIPD. The model displays the pseudo-centrosymmetry of the PIPD molecule. The chemistry involved in the synthesis of PIPD requires that the pyridinylene-N and CH present in the PIPD repeat unit may be interchanged going from one repeat unit to the next, which implies that parallel or antiparallel packing of chains in the crystal need not be considered since N and CH are distributed randomly over two positions in the unit cell. This may be incorporated into the model by the assigning of site occupation factors 0.5 to N and CH placed at both positions, after which the model will be centrosymmetrical. Note that in terms of electron density the difference between the pseudo-centrosymmetrical model and the centrosymmetrical model is so small that it does not influence the X-ray scattering intensities at all.

With the unit cell parameters known, the structure is completely determined by two positional parameters, i.e.

Table 1 Indexing of reflections and comparison of observed and calculated diffraction patterns of HT PIPD. The intensities are calculated based on the monoclinic model, assuming symmetric transmission geometry. The Lorentz and polarization factors are included in the calculated intensities as well as the reflection multiplicity. An overall isotropic temperature parameter of 4.0 Å^2 was assumed. Explanation: 2θ is the diffraction angle using CuKα radiation; vs = very strong, s = strong, m = medium, w = weak, diff = diffuse, — = not above background (which may be streaky)

$2\theta^{obs}$ (°)	$2\theta^{calc}$ (°)	d^{calc} (Å)	*h*	*k*	*l*[a]	I^{obs}	I^{calc}
14.82	14.83	5.974	2	0	0	s	489.4
26.69	26.71	3.338	1	1	0		1000.0
	29.74	3.004	2	1	0	vs	21.5
	29.92	2.987	4	0	0		11.4
45.16	45.56	1.991	6	0	0	vw	5.4
	46.10	1.969	5	1	0		4.2
52.63	52.66	1.738	0	2	0	w–diff	29.4
55.41	55.03	1.669	2	2	0		5.3
	14.38	6.157	− 2	0	1	—	5.4
18.64	18.85	4.709	2	0	1	m	17.0
	27.16	3.283	− 1	1	1	—	5.4
	28.53	3.129	1	1	1	[b]	10.2
32.80	33.35	2.687	4	0	1	vw	7.3
	33.47	2.678	− 3	1	1		6.4
	43.58	2.077	− 6	0	1	—	4.1
15.56	15.57	5.693	0	0	2	w	11.5
17.79	17.77	4.990	− 2	0	2	m–s	23.3
	24.80	3.590	2	0	2	—	6.5
28.90	29.00	3.079	− 4	0	2		25.8
	29.80	2.998	− 1	1	2	m–s	7.6
	32.27	2.774	1	1	2		10.9
	34.57	2.594	− 3	1	2	—	4.5
	44.57	2.033	− 5	1	2	—	4.5
23.38	23.43	3.797	− 2	0	3	s–m	74.6
	37.42	2.403	− 3	1	3	—	5.7
43.51	44.12	2.052	− 6	0	3		4.7
	44.15	2.051	4	0	3	w–diff	6.2
	46.02	1.972	− 5	1	3		9.2
	58.17	1.586	5	1	3	—	5.4
46.30	46.60	1.949	− 6	0	4	vw	4.0
37.44	37.52	2.397	− 2	0	5	s	429.3
	41.51	2.175	− 4	0	5		6.7
	46.22	1.964	− 1	1	5		12.4
	50.49	1.808	1	1	5		4.4
	52.89	1.731	− 5	1	5		4.8
45.30	45.30	2.002	− 2	0	6	s–m	135.2
	53.36	1.717	− 3	1	6		6.9

[a]The intensity of reflection $h\bar{k}l$ is taken into account via the reflection multiplicity, i.e. the intensity of reflection *hkl* includes that of $h\bar{k}l$
[b]Reflection 111 cannot be observed due to the neighbouring strong 110 reflection

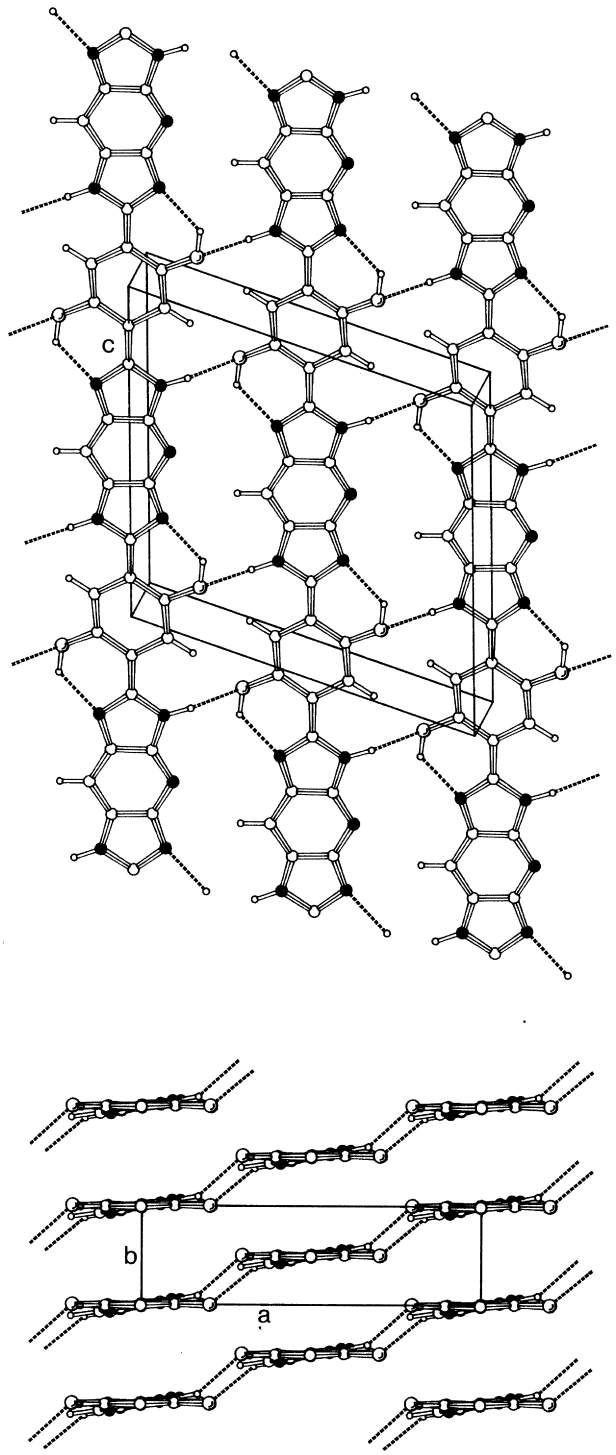

Figure 5 Triclinic model of HT PIPD showing hydrogen bonded sheets (approximately) parallel to the $(1\bar{1}0)$ planes. The upper picture shows the polymer chains at the (x, y) positions (0, 0), (1/2, 1/2), and (1, 1). The polymer chains at the corners and centre are related by c-centering. Nitrogen atoms are coloured black, oxygen atoms are drawn somewhat larger to discriminate them from carbon atoms. The pyridinylene-N and -CH may be interchanged randomly

the angles of the planar dihydroxyphenyl and heterocyclic fragments with the *ac*-plane of the unit cell (the difference of these angles being the torsion angle between the planar fragments). The model was optimized by a combination of diffraction pattern matching (i.e. by comparing calculated diffraction patterns with the observed diffraction pattern) and energy minimization. Energy minimization was performed using the Dreiding II force field[18] with electrostatic interactions taken into account via Gasteiger[19] charges. In the minimization the cell parameters were kept fixed. Note that optimization of the two parameters based solely on XRD data suffers from the relatively low crystalline perfection of the material which limits the accuracy of the parameters. It was found that the dihydroxyphenyl fragment is parallel to the *ac*-plane, whereas the heterocyclic fragment is slightly rotated. Subsequent analysis of interatomic distances suggested the presence of a hydrogen bonding scheme containing intermolecular N–H—O hydrogen bonds and intramolecular O–H—N hydrogen bonds (*Figure 5*). The interchain N–H—O bonds connect the shifted polymer chains, forming hydrogen bonded sheets running along one of the diagonals of the projection unit cell. The intramolecular hydrogen bonds are located between the rigid fragments and thus contribute to the rigidity of the chains.

Comparing the projection unit cell of PIPD with that of PBO it is tempting to conclude that the two-chain projection unit cell of PIPD is rectangular as a result of identical interactions (i.e. hydrogen bonds) along the diagonals. This suggests that the sheet-like model needs modification, as it is not compatible with the latter conclusion (unless we assume a disorder model with sheets running on average along both diagonals). The fact that the diffraction pattern calculated on the basis of the sheet-like model closely corresponds to the observed diffraction pattern implies that the difference in positional parameters of the centre chain with respect to those of the corner chain in the two-chain unit cell must be small. This requirement and that of identical diagonals is fulfilled if the centre and corner chains are related by the monoclinic symmetry operation $x + 1/2$, $-y + 1/2$, z, associated with an a-glide plane perpendicular to the b-axis, instead of by the c-centering symmetry operation $x + 1/2$, $y + 1/2$, z.

In the monoclinic model the same two positional parameters remain to be optimized as in the sheet-like model. The angles of the two rigid fragments with the *ac*-plane were found to be equal in magnitude as compared to those in the triclinic model, the only difference being that the sign of the angle of the heterocyclic fragment of the corner chain is opposite to that of the centre chain. Intermolecular distance analysis indicated the presence of a bi-directional hydrogen bonding network in which each polymer chain is linked to its four axially shifted neighbours by N–H–O hydrogen bonds (*Figure 6*). Intramolecular O–H–N bonds are proposed to be present between the rigid fragments similar to those in the triclinic model. The space group of the model is monoclinic, *Pa* (pseudo-$P2_1/a$) with its unique axis (i.e. the b-axis) perpendicular to the fibre axis. If the random distribution of pyridinylene-N and CH is incorporated into the model we can drop the prefix 'pseudo', for then the symmetry requirements of the centrosymmetric space group $P2_1/a$ are fulfilled.

The fractional atomic coordinates of the triclinic and monoclinic models are listed in *Table 2*. As the polymer chains located at the centre and corners of the projection unit cell are related by c-centering and a-glide symmetry, respectively, it is possible in principle to discriminate between the two models via the extinction rules associated with the latter symmetry elements. The c-centering operation produces systematically absent reflections hkl for $h + k$ odd, whereas a-glide symmetry generates systematic absences $h0l$ with h odd. Therefore, the presence of e.g. the reflection 010 indicates a-glide symmetry and rules out the c-centered model. However, the relatively small

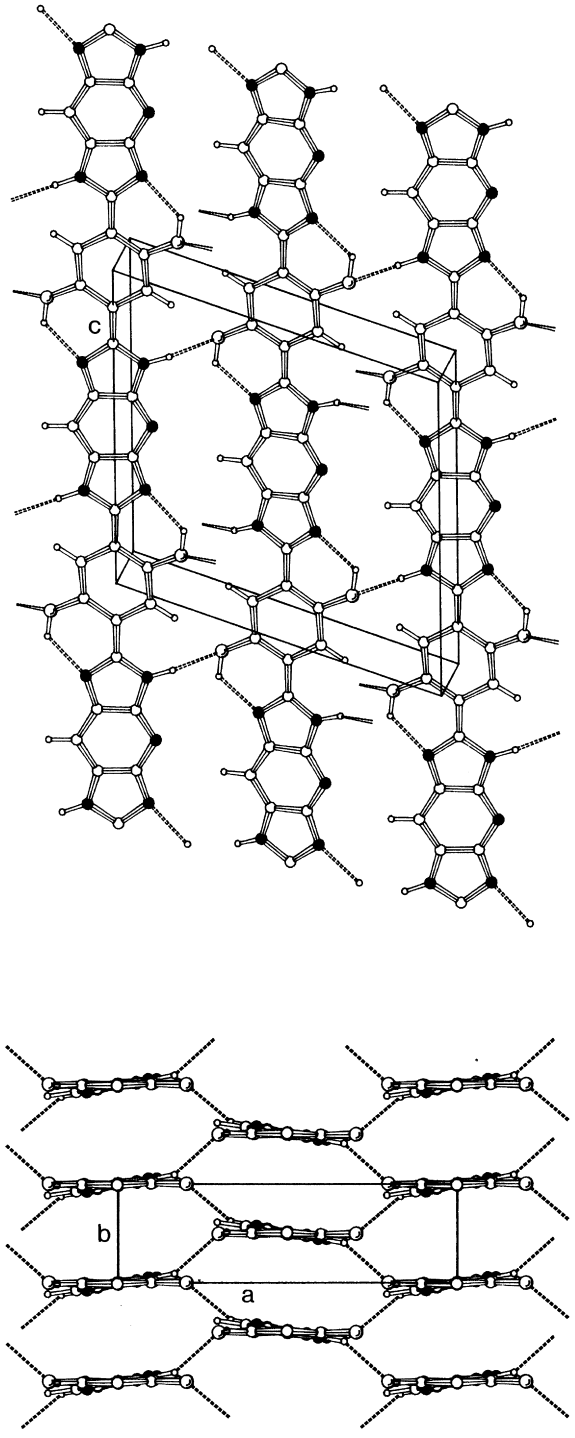

Figure 6 Monoclinic model of HT PIPD with bi-directional hydrogen bonding network. The picture differs from that in *Figure 5* in that the *c*-centering is replaced by *a*-glide symmetry. Note that the dihydroxyphenyl moiety of the centre chain forms hydrogen bonds along the (1$\bar{1}$0) planes (just like in *Figure 5*), while the heterocyclic moiety forms hydrogen bonds along the (110) planes

differences in positional parameters between the two models translate into only small diffraction pattern differences. The quality of the observed diffraction patterns as determined by the degree of crystalline perfection is at present not high enough to allow discrimination between the two models along these lines.

Using in-house built software, diffraction intensities were calculated based on the two models, assuming symmetric transmission geometry. In view of the small differences between the diffraction patterns corresponding to the two models, we will only present intensity calculations based on the monoclinic model (*Table 1*). *Figure 2* compares the observed flat-plate diffraction pattern with that simulated by the Cerius2 software. The latter pattern not only very clearly shows the four relatively strong characteristic off-axis spots on the first three layer lines but much weaker spots are present as well. Three of the four strong off-axis spots are indexed as 201, $\bar{2}$02, and $\bar{2}$03, whereas the remaining spot on the second layer line is a composite reflection, its main contribution being indexed as $\bar{4}$02 (*Table 1*). The strong $\bar{2}$05 reflection close to the meridian is not very well represented on the calculated flat-plate pattern. This part of the diffraction pattern is more difficult to simulate due to the curvature of the Ewald sphere. In symmetric transmission geometry the calculated meridional diffraction pattern (*Figure 7*) very clearly shows the $\bar{2}$05 reflection. The results in *Table 1* and *Figures 2* and *7* show that the differences between observed and calculated diffraction patterns are relatively small. Considering that the layer line streaking that is present in the observed diffraction pattern is not taken into account in the calculated diffraction patterns, it is concluded that the observed diffraction patterns are well explained by the proposed model(s).

The hydrogen bonding geometry of the models is summarized in *Table 3*. The hydrogen bond lengths and D–H—A angles in the triclinic model are (practically) identical to those in the monoclinic model. From *Table 3* it is concluded that the models show acceptable hydrogen bonding schemes.

It is instructive to consider the isolated chain conformation of PIPD as obtained via the Cerius2 program. For this purpose six PIPD repeat units were linked into a polymer chain that was subsequently optimized using the Dreiding II force field[18]. In the resulting conformation, the torsion angles between the rigid dihydroxyphenyl and heterocyclic

Table 2 Fractional atomic coordinates of the corner chain referred to the two-chain unit cell; the coordinates of the second chain are given by $x + 1/2$, $y + 1/2$, z for the triclinic model, and $x + 1/2$, $-y + 1/2$, z for the monoclinic model

Atom	*x*	*y*	*z*
O1	0.202	0.002	0.167
O2	−0.203	0.003	−0.165
N1	0.114	0.051	0.540
N2	0.089	0.052	0.732
N3	−0.094	−0.044	0.675
N4	−0.092	−0.073	0.269
N5	0.090	0.032	0.331
C1	0.055	0.026	0.616
C2	−0.001	0.009	0.768
C3	−0.061	−0.035	0.581
C4	−0.123	−0.073	0.462
C5	−0.061	−0.048	0.385
C6	0.055	0.015	0.424
C7	0.000	−0.018	0.236
C8	−0.002	−0.009	0.119
C9	0.097	0.006	0.088
C10	0.104	0.017	−0.025
C11	0.000	0.008	−0.115
C12	−0.099	−0.001	−0.085
C13	−0.106	−0.008	0.029
H1	0.212	−0.016	0.251
H2	−0.213	0.003	−0.249
H3	0.166	0.096	0.779
H4	−0.167	−0.125	0.219
H5	0.177	0.030	−0.044
H6	−0.180	−0.014	0.048
H7	−0.207	−0.115	0.435

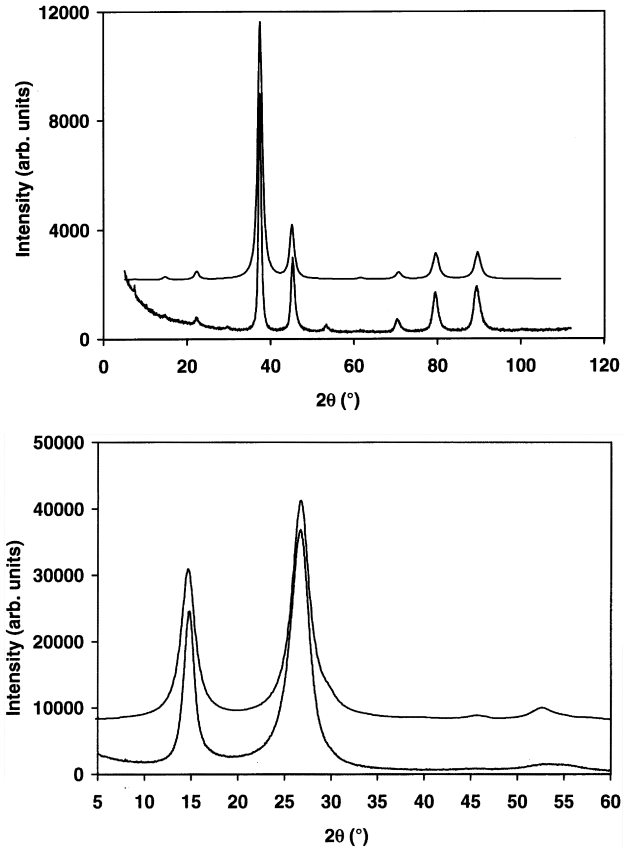

Figure 7 Observed (bottom curve) *versus* calculated (upper curve) X-ray scattering of HT PIPD fibre, upper diagram meridional scattering, lower diagram equatorial scattering

Table 3 Hydrogen bonding geometry of the monoclinic model (which is practically identical to that of the triclinic model): D = hydrogen bond donor; A = hydrogen bond acceptor

Type	D–H—A	D—A (Å)	H—A (Å)	D–H—A (°)
Inter	N–H—O	2.95	2.10	146
Inter	N–H—O	2.91	2.04	148
Intra	O–H—N	2.76	2.06	127
Intra	O–H—N	2.70	2.00	127

fragments were almost zero after minimization, i.e. the two fragments were practically coplanar in each repeat unit. An intramolecular O–H—N hydrogen bond was found to exist between each dihydroxyphenyl and heterocyclic fragment. The polymer chains in the triclinic and monoclinic models have a torsion angle of 8.1°. This means that intermolecular interactions lead to a twist of the polymer chains. An increase in torsion angle leads to an energetically unfavourable decrease in conjugation of the polymer. In the monoclinic model this effect is opposed by a decrease in hydrogen bond lengths which may be energetically favourable.

Energy minimization of the two models, using the Dreiding II force field[18] with Gasteiger[19] charges, resulted in total energies of 48.7 and 50.8 kcal mol^{-1} for the triclinic and monoclinic structures, respectively. In these minimizations the unit cell parameters were not fixed. In view of the small energy difference it is impossible to discriminate between the two models via these energy calculations. Preliminary *ab initio* molecular dynamics calculations (Car–Parinello method) did not afford a means of discriminating between the two models either, as both models were found to be minimum energy structures, the energy difference being negligible[20,21].

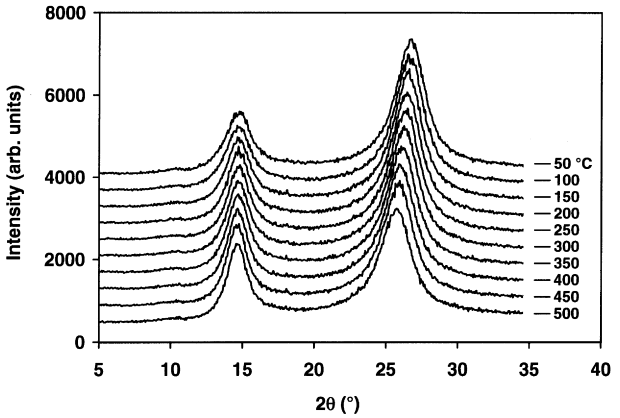

Figure 8 Equatorial X-ray scattering of HT PIPD fibre as function of temperature

Thermal expansion

Since the two models for HT PIPD differ in the intermolecular interactions along the diagonals of the two-chain unit cell, thermal expansion data as obtained from high temperature XRD measurements can provide valuable insight. If the sheet-like model is correct, these interactions are not identical and we would expect different coefficients of thermal expansion for the (110) and (1$\bar{1}$0) planes. In other words, we would expect a splitting of the 3.34 Å peak in the equatorial diffraction pattern with temperature. *Figure 8* shows the equatorial X-ray scattering of HT PIPD measured in reflection geometry upon heating from 50 to 550°C. Clearly, there is no sign of any splitting of the 3.34 Å reflection in the entire temperature range. We therefore conclude that the monoclinic model with its bi-directional hydrogen bonding scheme is consistent with thermal expansion data, whereas the triclinic sheet-like model is not.

Throughout the temperature range the projection unit cell remains rectangular as no splitting of the combined 110 and 1$\bar{1}$0 peak is observed. The material shows a progressive shift of this peak to lower diffraction angle with temperature, unlike the 200 peak which hardly shifts at all. These observations imply that the projection unit cell expands almost exclusively along the *b*-axis. This can be explained as a consequence of temperature induced rotation (libration) of the polymer chains around their axes, which in view of the ellipsoidal cross-section of the chains leads to an expansion of the unit cell along the *b*-axis. An increase in the torsion angle between the rigid fragments also leads to unit cell expansion along the latter axis. However, this effect will be less favourable as it will lower the conjugation of the polymer chains along their axes.

XRD ANALYSIS OF AS-SPUN PIPD FIBRE

Figure 9 displays the flat-plate X-ray diffraction pattern of as-spun PIPD fibre. The diffraction pattern shows rather large differences compared to that of the heat-treated fibre. In contrast to the heat-treated fibre, reflections indicating three-dimensional order are not observed. Both as-spun and heat-treated PIPD fibre exhibit a reflection at about 3.3 Å (3.32 and 3.34 Å, respectively), but the second strong reflection corresponds to a spacing of 8.38 Å for as-spun PIPD compared to 5.98 Å for heat-treated PIPD (*Figure 10*).

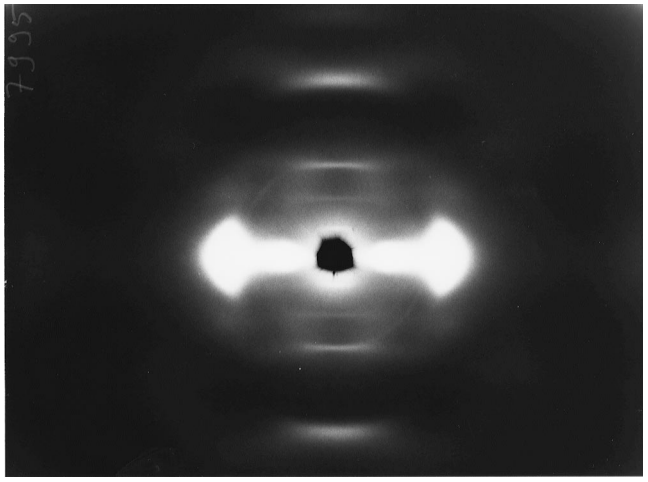

Figure 9 Flat plate X-ray diffraction pattern of as-spun PIPD fibre

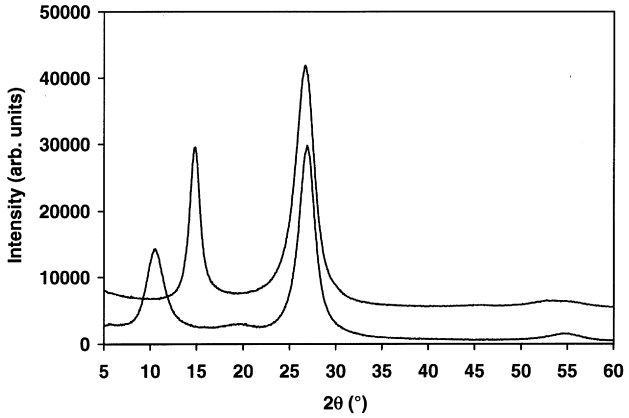

Figure 10 Equatorial X-ray scattering of as-spun PIPD fibre (bottom curve) and heat-treated PIPD fibre (upper curve)

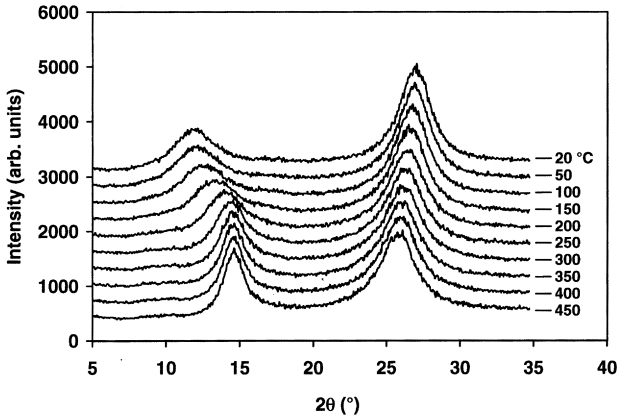

Figure 11 Equatorial X-ray scattering of as-spun PIPD fibre as function of temperature in a nitrogen atmosphere

Low intensity reflections are observed in the diffraction pattern of as-spun PIPD at spacings of 4.56 and 1.68 Å.

Figure 11 shows the changes in the equatorial X-ray scattering of as-spun PIPD fibre upon heating from room temperature to 500°C in a nitrogen atmosphere. Over this temperature range the material shows a progressive shift of the 3.32 Å reflection to smaller angle (i.e. larger spacing), which is attributed to thermal expansion. In the temperature range from room temperature to 300°C the 8.38 Å reflection

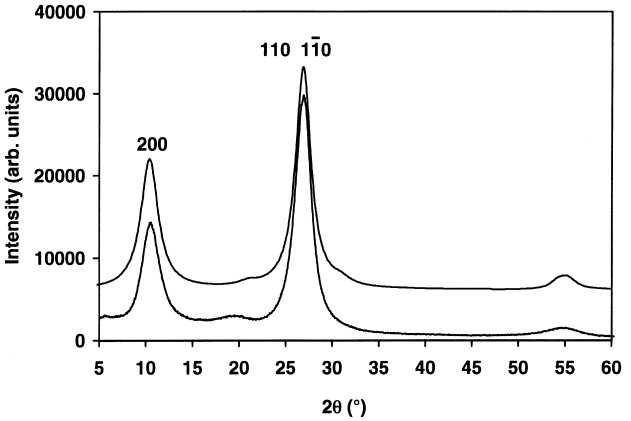

Figure 12 Observed (bottom curve) and calculated (upper curve) equatorial X-ray scattering of as-spun PIPD fibre

gradually shifts to larger angle (i.e. smaller spacing), suggesting that the material undergoes a change in structure. At higher temperatures the position of the latter reflection does not change and the high temperature scan has become identical to that of heat-treated PIPD fibre shown in *Figure 8*. Treatment of as-spun PIPD with dry nitrogen also produces a shift of the 8.38 Å reflection to smaller spacings. In the latter case the structural change associated with the peak shift is reversible since, after exposing the fibre to ambient conditions, the shifted peak returns to its initial position. This reversibility is also observed if the as-spun material is subjected to a relatively mild heat treatment.

The observations described above indicate that the as-spun structure is a two-dimensionally ordered hydrate. In this hydrate the polymer chains are packed regularly in lateral directions, but they lack longitudinal register. Upon heating or treatment with dry nitrogen, a structural transition takes place during which the hydrogen bonded water molecules, located between the polymer chains, are removed from the hydrate. The two-dimensional packing of the polymer chains in the hydrate can be described with a rectangular unit cell with dimensions $a = 16.85$ Å, $b = 3.38$ Å, containing polymer chains at its corners and centre.

A model of the as-spun structure was constructed by placing planar polymer chains at the corners and centre of a unit cell with dimensions $a = 16.85$ Å, $b = 3.38$ Å, $c = 12.01$ Å. Observed and calculated (equatorial) intensities are in reasonable agreement if the plane of the polymer chains is parallel to the *ac*-plane, and with eight water molecules placed in the unit cell at positions $x = 1/4\ (+1/2)$, $y = 1/4\ (+1/2)$ so that each (x, y) position is occupied by two water molecules having different *z*-coordinates. Since the as-spun structure shows axial disorder, the latter coordinates are undetermined and only the *ab*-projection of the model is meaningful. *Figure 12* shows observed and calculated diffraction patterns. An anisotropic disorder parameter with a root mean square value of 0.6 Å^2 in the *a* direction was introduced in the diffraction calculation, in order to lower the intensities of three reflections (with indices 400, 310, and 600), which are not present in the observed diffraction pattern.

In the resulting PIPD.4H2O model, layers of polymer molecules packed face to face in the *b* direction alternate with layers of hydrogen bonded water molecules (*Figure 13*). The calculated density is 1.60 g cm^{-3}. While this model contains 21.4 wt% water molecules, the observed

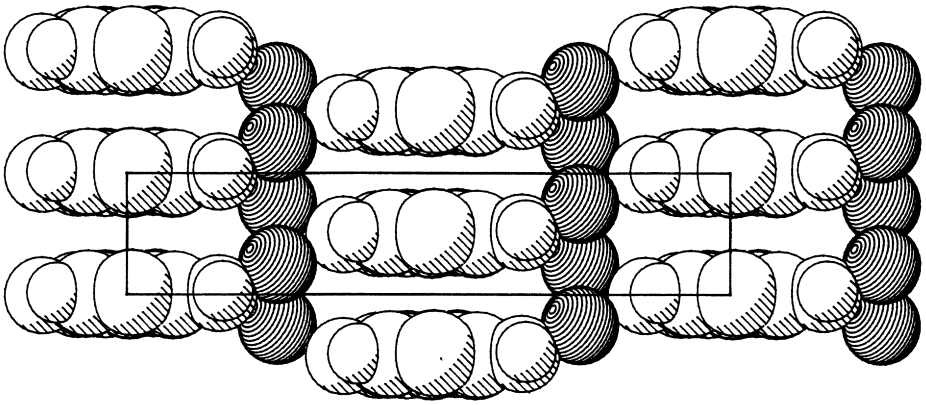

Figure 13 Projection down the *c*-axis of the model of as-spun PIPD. The atoms are drawn with radii equal to 0.7 times their Vanderwaals radii. The oxygen atoms of the water molecules are dark coloured. Their hydrogen atoms have been omitted

weight loss due to heat treatment of as-spun PIPD ranges from 18 to 23 wt%. Taking into account that this weight loss includes water molecules originating both from the crystal lattice and from voids in the material, the actual water content of the hydrate may be somewhat lower than four water molecules per PIPD repeat. A comparison of the lattice of the heat-treated structure with that of the as-spun structure shows that heat treatment results in a 27% decrease in unit cell cross-section.

The low intensity reflection at 4.56 Å is not explained by the model. While this reflection is present in the XRD pattern of as-spun PIPD in *Figure 10*, it is absent from the multi-temperature XRD scan in *Figure 11* (even from the scan at 20°C), the difference being that the former measurement was conducted at ambient conditions whereas the latter was conducted in a nitrogen atmosphere. Since the reflection disappears within minutes after exposure of the material to (dry) nitrogen, it is not present in the multi-temperature scan in *Figure 11*.

We have seen that the 200 reflection shifts as a result of dehydration or hydration. Its spacing varies continuously between between 6.0 and 8.4 Å depending on the degree of hydration. In a two-phase model of partly dehydrated material, made up of hydrated and water-free domains, one would expect a peak at 6.0 Å and a second peak at 8.4 Å, rather than a single peak somewhere between 6.0 and 8.4 Å. Since a unit cell with a variable size is not a likely explanation for this observation, we now focus attention on a lattice disorder model. Consider an as-spun crystallite, its (200) planes spaced 8.4 Å apart, with water molecules between them. At the onset of dehydration, water molecules are lost from the crystallite and the distance between some of the (200) planes in the crystallite will be 6.0 Å, instead of 8.4 Å. Hence, in the *b* direction we have a lattice of two different repeat units instead of one. The 6.0 Å spacings are distributed randomly throughout the crystallite. The position of the 200 reflection in the diffraction pattern is determined by the function that describes the distribution of 6.0 Å and 8.4 Å spacings. This distribution function changes with increasing dehydration as more and more 8.4 Å spacings are replaced by 6.0 Å spacings. The continous change of the distribution function leads to the continous shift of the 200 reflection. A theoretical description of a continuous peak shift, based on a random distribution of two discrete spacings, was given more than 60 yrs ago in a paper by Hermans[22]. In this treatment, which did not receive wide attention, Hermans derived the interference function for a one-dimensional lattice with liquid-like (later called 'paracrystalline') distortions with bimodal coordination statistics.

A random distribution of two repeat units is also encountered in a different context, *viz*. in that of random copolymers built of two types of monomers that differ in molecular length. Blackwell *et al*.[23] have studied the diffraction patterns of stiff chain liquid crystalline aromatic copolyesters. The meridional diffraction patterns were consistent with models for stiff chains of random monomer sequences. It was found that the meridional reflections shift in position, depending on the monomer ratio. Since the monomer ratio determines the fraction of the two different repeat units, it plays the same role as the degree of hydration in the case of PIPD. The interference function of Blackwell *et al*.[23] for the copolymer case is a generalization of the interference function derived by Hermans[22].

In summary, as-spun PIPD is a hydrate. Partly dehydrated as-spun PIPD can be described by a lattice disorder model, as described above. Heat treatment of as-spun PIPD initially (i.e. up to 300°C) leads to decomposition of the hydrate and, at sufficiently high temperatures, to the development of three-dimensional crystalline order, characteristic of the heat-treated crystal structure.

DISCUSSION

Two models were presented for the crystal structure of HT PIPD, containing either hydrogen bonded sheets (triclinic model) or a bi-directional hydrogen bonding network (monoclinic model). Based on thermal expansion data the interactions along the diagonals of the two-chain projection unit cell were found to be identical, implying that the triclinic sheet-like model must be abandoned in favour of the monoclinic model.

As was noted before, energy minimization using the Dreiding II[18] forcefield and ab initio molecular dynamics calculations show that the energy difference between the triclinic and monoclinic models is small[20,21]. Although the triclinic sheet-like model is not consistent with high temperature data, the presence of hydrogen bonded sheets can be reconciled with these data by the assumption of a (disorder) model where the sheets run on average along both diagonals of the two-chain unit cell. It is not difficult to imagine sheet-like distorsions in a monoclinic model. Such a model can also be described as a hybrid model consisting of both triclinic and monoclinic domains within a single crystallite. The average two-chain unit cell of the latter disorder model has identical interactions along its diagonals

and can still be described as containing a bi-directional hydrogen bonding network.

It was shown that the key interchain interaction in HT PIPD fibre is N–H—O hydrogen bonding between axially shifted polymer chains. Apart from intermolecular bonding the hydroxyl groups in HT PIPD also take part in intramolecular hydrogen bonding via O–H—N bonds. This was confirmed by *ab initio* molecular dynamics calculations[20,21]. Based on spectroscopic evidence Tan *et al.*[6] concluded that the latter type of hydrogen bonding is also present in dihydroxy-PBZT. This conclusion was supported by the observation that the presence of hydroxyl groups did not result in any improvement of its compression performance.

Although the pyridinylene-N atom can act as a hydrogen bond acceptor, it does not take part in the hydrogen bonding network in HT PIPD (it may however do so in as-spun PIPD). Therefore, it is expected that the PIPD analog with the pyridinylene-N atom replaced by a carbon atom has the same crystal structure after heat treatment as HT PIPD. The latter analog, known as dihydroxy-PBI[24], is based on 2,5-dihydroxyterephthalic acid and 1,2,4,5-tetraaminobenzene. High molecular weight polymer, obtained via the 1:1 complex of the latter two materials[7], was spun into fibres. X-ray diffraction patterns of both as-spun and heat-treated fibres were subsequently recorded and found to be very similar to those of as-spun and heat-treated PIPD, respectively. Therefore, the crystal structures of the two polymers are practically identical, i.e. as-spun dihydroxy-PBI is a hydrate that decomposes upon heat treatment to form the monoclinic water-free crystal structure. Our conclusion that dihydroxy-PBI can form a hydrate is in line with results by Dang *et al.*[24], who report that the material has a strong affinity for water. Note that dihydroxy-PBI, being less polar than PIPD, shows a reduced solubility in PPA as compared to PIPD (8–9 wt% *versus* 20 wt%)[7]. Hence, its properties are not comparable to those of PIPD, despite the similarity in crystal structure.

The design of the PIPD polymer was aimed at introducing strong interactions between the polymer chains in order to achieve good compression properties[7]. The shear modulus and compression strength of HT PIPD fibre were found to be 7.4 GPa and 1.7 GPa, respectively[16]. These, for polymer fibres exceptionally high values are satisfactorily explained by the proposed monoclinic structure with its bi-directional hydrogen bonding network (possibly with sheet-like distorsions).

As noted already, the two-chain projection unit cell describing the lateral packing of HT PBO is oblique, whereas that of HT PIPD is rectangular. The *ab*-plane of the unit cell of HT PIPD is not perpendicular to the *c*-axis (chain axis) resulting in a *c*-axis shift of 2.0 Å (0.17*c*) of neighbouring polymer chains. The packing of polymer chains in HT PBO was described in a two-chain monoclinic unit cell by Fratini *et al.*[14] and Martin and Thomas[12], the *ab*-plane of the unit cell being perpendicular to the *c*-axis (chain axis). According to the latter authors, neighbouring chains exhibit disorder in that they are shifted randomly by $+1/4c$ or $-1/4c$. The random $\pm 1/4c$ shift of PBO polymer chains contrasts with the regular (i.e. non-random) 2.0 Å shift of polymer chains in HT PIPD. Hence, HT PIPD has a higher three-dimensional order than HT PBO, which is attributed to the presence of the hydrogen bonding network.

Sweeney[3] examined crosslinking in halogenated PBZT fibres as a function of heat treatment time and temperature, the method of crosslinking being based on the coupling of free radicals formed by thermolysis of active aryl halides contained in the polymer unit. The degree of crosslinking, which determines the compression performance, increases with the temperature and duration of the heat treatment, the elimination of halogens being relatively slow. In his study Sweeney reported some improvement in compression performance, but this was accompanied by a loss of tensile properties, which according to the author may be caused by the formation of voids created in the elimination of the halogen atoms. In the same study, an X-ray diffraction pattern of PBZBrT heat-treated for 10 s at 400 or 500°C was presented without interpretation in terms of crystal structure. Surprisingly, the latter diffraction pattern is similar to that of HT PIPD (although details are difficult to assess from the printed diffraction pattern). This implies that the three-dimensional register of polymer chains in PBZBrT is comparable to that in HT PIPD. It remains to be examined if this three-dimensional register is retained after crosslinking via halogen elimination (diffraction patterns of crosslinked material were not reported). Note that in either case the degree of crosslinking and the perfection of the structure may differ considerably from those in HT PIPD.

It is interesting to compare the hydrogen bonding in PIPD with that in cellulose. In native cellulose (cellulose I) the molecular chains are arranged in hydrogen bonded sheets, whereas regenerated cellulose (cellulose II) contains a bi-directional hydrogen bonding network[25]. Unlike the cellulose I lattice, the cellulose II lattice is accessible by water molecules. The existence of a hydrate of cellulose was reported some 60 yrs ago[26]. This hydrate was obtained by cold washing of mercerized cellulose (cellulose treated with a solution of sodium hydroxide). According to Hermans and Weidinger[27] the same hydrate is found in freshly regenerated cellulose. The hydrate is unstable and decomposes slowly (rapidly when heated and dried) to form a second hydrate with a lower water content, the latter hydrate being stable. In the X-ray diffraction pattern this decomposition is accompanied by the gradual shift of an equatorial reflection from a spacing of 8.98 Å to 7.73 Å[26,27] very similar to the shift of the 200 reflection of as-spun PIPD.

CONCLUSIONS

The wide angle X-ray diffraction pattern of HT PIPD shows characteristic off-meridian reflections on the lower order layer lines, which exhibit no significant meridional scattering. The first observation indicates three-dimensional crystalline order, whereas the latter indicates that the *ab*-plane of the unit cell is not perpendicular to the *c*-axis.

A procedure of unit cell determination was introduced that made it possible to index the diffraction pattern and find the three-dimensional packing. The packing can be described by a non-primitive unit cell with cell dimensions 12.60, 3.48, 12.01 Å, 90.0, 108.6, 90.0°. The two-dimensional projection cell describing the lateral packing is rectangular and contains two polymer chains located at its centre and corners. The calculated density is 1.77 g cm^{-3}. As the *a*-axis is not perpendicular to the chain axis (*c*-axis), neighbouring chains packed along the diagonals of the projection cell are shifted relative to each other in the direction of the *c*-axis by 2.0 Å. This regular *c*-axis shift explains the observed absence of significant meridional scattering from the lower order layer lines of the diffraction pattern.

The proposed crystal structure of HT PIPD has $P2_1/a$ symmetry and contains intermolecular N–H—O hydrogen bonds and intramolecular O–H—N bonds. The

intermolecular N–H—O bonds form a bi-directional hydrogen bonding network in which each polymer chain is linked to its four axially shifted neighbours. The intramolecular O–H—N bonds contribute to the rigidity of the polymer chains. The intermolecular hydrogen bonding scheme is consistent with thermal expansion data obtained via high temperature X-ray diffraction, which show that the interactions along the diagonals of the projection unit cell (i.e. parallel to the (110) and $(1\bar{1}0)$ planes) are identical. A triclinic model containing hydrogen bonded sheets running along one of the diagonals of the projection unit cell is not consistent with thermal expansion data. It is concluded that sheets may be present in a disorder model, e.g. a monoclinic model with sheet-like distorsions. To be consistent with the thermal expansion data, the disorder model must not only contain sheets running parallel to the $(1\bar{1}0)$ planes but also sheets running parallel to the (110) planes.

The regular (i.e. non-random) *c*-axis shift of polymer chains in HT PIPD contrasts with the random $\pm 1/4c$ shift of polymer chains in HT PBO. Hence, the former material has a higher three-dimensional order than the latter, as a result of the presence of the hydrogen bonding network.

The monoclinic crystal structure with its bi-directional hydrogen bonding network (possibly with sheet-like distortions) provides a satisfactory explanation for the exceptionally good compression performance of heat-treated PIPD fibre.

The structure of as-spun PIPD can be characterized as a two-dimensionally ordered hydrate. In this hydrate the polymer chains are packed regularly in lateral directions, but they lack longitudinal register. The two-dimensional packing of the polymer chains in the hydrate was described with a rectangular unit cell with dimensions $a = 16.85$ Å, $b = 3.38$ Å, containing planar polymer chains at its corners and centre. Layers of polymer molecules packed face to face are separated by layers of hydrogen bonded water molecules.

Upon heating, the water is removed from the structure and the hydrate decomposes. The spacing of the 200 reflection varies with the degree of hydration, and shifts progressively from 8.4 to 6.0 Å during heat treatment. This continuous shift can be explained in terms of a lattice disorder model assuming a random distribution of two repeat units in the *a* direction. At sufficiently high temperatures all water molecules are lost from the structure and the bi-directional hydrogen bonding network is developed that is characteristic of the heat-treated crystal structure with its three-dimensional crystalline order.

ACKNOWLEDGEMENTS

The stimulating interest of Drs Doetze Sikkema and Maurits Northolt in the present study is greatfully acknowledged.

REFERENCES

1. Adams, W. W., Eby, R. K. and McLemore, D. E., *The materials science and engineering of rigid rod polymers. Mat. Res. Soc. Symp. Proc.*, 1989, **134**.
2. Allen, S. R., *J. Mat. Sci.*, 1987, **22**, 853.
3. Sweeny, W., *J. Pol. Sci.*, 1992, **A30**, 1111.
4. Sahafeyan, M. and Kumar, S., *J. Appl. Pol. Sci.*, 1995, **56**, 517.
5. Mehta, V. R., Kumar, S., Polk, M. B., Vanderhart, D. L., Arnold, F. E. and Dang, T. D., *J. Pol. Sci.*, 1996, **B34**, 1881.
6. Tan, L.-S., Arnold, F. E., Dang, T. D., Chuah, H. H. and Wei, K. H., *Polymer*, 1994, **35**, 3091.
7. Sikkema, D. J., *Polymer*, 1998, **39**(24), 5981–5986.
8. Roche, E. J., Takahashi, T. and Thomas, E. L., in *Fiber Diffraction Methods*, Vol. 141, eds A. D. French and K. H. Gardner. ACS Symp. Ser., 1980, p. 303.
9. Odell, J. A., Keller, A., Atkins, E. D. T. and Miles, M. J., *J. Mater. Sci.*, 1981, **16**, 3309.
10. Shimamura, K., Minter, J. R. and Thomas, E. L., *J. Mater. Sci. Lett.*, 1983, **2**, 54.
11. Krause, S. J., Haddock, T. B., Vezie, D. L., Lenhert, P. G., Hwang, W.-F., Price, G. E., Helminiak, T. E., O'Brien, J. F. and Adams, W. W., *Polymer*, 1988, **29**, 1354.
12. Martin, D. C. and Thomas, E. L., *Macromolecules*, 1991, **24**, 2450–2460.
13. Adams, W. W., Kumar, S., Martin, D. C. and Shimamura, K., *Polymer Com.*, 1989, **30**, 285.
14. Fratini, A. V., Lenhert, P. G., Resch, T. J. and Adams, W. W., *The materials science and engineering of rigid rod polymers. Mat. Res. Soc. Proc.*, 1989, **134**, 431–445.
15. Martin, D. C., *Macromolecules*, 1992, **25**, 5171.
16. Lammers, M., Klop, E. A., Northolt, M. G. and Sikkema, D. J., *Polymer*, 1998, **39**(24), 5999–6005.
17. Van 't Spijker, E., personal communication.
18. Mayo, S. L., Olafson, B. D. and Goddard, W. A., *J. Phys. Chem.*, 1990, **94**, 8897–8909.
19. Gasteiger, J. and Marsili, M., *Tetrahedron*, 1980, **36**, 3219.
20. van der Horst, J. W., M.Sc. thesis, Nijmegen University, The Netherlands, 1997.
21. Hageman, J. C. L., van der Horst, J. W. and de Groot, R. A., *Polymer*, in press.
22. Hermans, J. J., *Rec. Trav. Chim.*, 1944, **63**, 211.
23. Blackwell, J., Biswas, A. and Bonart, C., *Macromolecules*, 1985, **18**, 2126–2130.
24. Dang, T. D., Tan, L. S. and Arnold, F. E., *Proc. ACS Pol. Mat. Sci. Eng.*, 1990, **62**, 86.
25. Kroon-Batenburg, L. M. J. and Kroon, J., *Carbohydrates in Europe*, 1995, **12**, 15–19.
26. Sakurada, I. and Hutino, K., *Kolloid-Z.*, 1936, **77**, 347.
27. Hermans, P. H. and Weidinger, A., *J. Coll. Sci.*, 1946, **1**(2), 185–193.